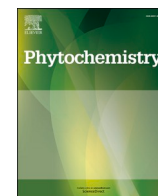




Contents lists available at ScienceDirect

## Phytochemistry

journal homepage: [www.elsevier.com/locate/phytochem](http://www.elsevier.com/locate/phytochem)Secotrijugins A–D, four highly oxidized and rearranged limonoids from *Trichilia sinensis* and their anti-inflammatory activityHonghong Xing<sup>a,1</sup>, Ziteng Song<sup>a,1</sup>, Ruichen Guo<sup>a,1</sup>, Feng Liu<sup>a,1</sup>, Lijun An<sup>a</sup>, Yuanqiang Guo<sup>a,\*\*</sup>, Ping Hu<sup>b,\*</sup><sup>a</sup> State Key Laboratory of Medicinal Chemical Biology, College of Pharmacy, and Tianjin Key Laboratory of Molecular Drug Research, Nankai University, Tianjin, 300350, China<sup>b</sup> Key Laboratory of Research on Pathogenesis of Allergen Provoked Allergic Disease in Liaoning Province, Shenyang Medical College, Shenyang, 110034, China

## ARTICLE INFO

## Keywords:

*Trichilia sinensis*  
Meliaceae  
Limonoids  
Anti-inflammatory activity

## ABSTRACT

Four undescribed highly oxidized and rearranged limonoids, secotrijugins A–D, were purified from the leaves and twigs of *Trichilia sinensis*. Within them, secotrijugin A was characterized as a rare 30-nortrijugin-type limonoid with an unusual cleavage of 1,14-ether bond, secotrijugins B and C represented new examples with the cleavage of  $\delta$ -lactone ring D, and secotrijugin D was a rare trijugin-type limonoid with an unusual 2,6-oxygen bridge. The structures of limonoids were characterized by means of spectroscopic analysis and ECD calculations. The cellular screening revealed that secotrijugin B was the most active against LPS-stimulated NO production in BV-2 cells, which played an anti-inflammatory role by downregulating COX-2 and iNOS protein expression. The further *in vivo* experiments confirmed that secotrijugin B had strong *in vivo* anti-inflammatory effect via suppressing NO and ROS generation.

## 1. Introduction

Limonoids, a class of bitter or juicy constituents of lemon or other citrus fruits and structurally regarded as tetranortriterpenoids possessing 17 $\beta$ -furan ring, are the typical phytochemicals of the plant Meliaceae family (Tan and Luo, 2011). With abundant structural scaffolds upon oxidations and skeletal rearrangements, together with multiple biological activities, such as insect antifeedant, anti-inflammatory, cytotoxic, and antibacterial effects, limonoids from the Meliaceae plant family have aroused great interest in the field of chemical and biological research around the world (Li et al., 2017, 2019; Liu et al., 2016; Lv et al., 2016; Sun et al., 2022; Tsukamoto et al., 2019; Zhang et al., 2022; Zhou et al., 2016; Zhu et al., 2019). Members of the genus *Trichilia* (Meliaceae) are well-known for biosynthesizing structurally diverse limonoids with an extensive spectrum of biological activities. There are about 86 species in the genus *Trichilia*, which are widely distributed in the tropics of America and Africa, India, Indo-China Peninsula, and

Malay Peninsula of Asia. Presently, three *Trichilia* species are found to grow in the southwest of China (Editorial Committee of the Flora of China, Chinese Academy of Sciences, 1997). Plenty of limonoids with different skeleton structures, such as havanensin-, trichilin-, mexicanolide-, phragmalin-, and trijugin-type limonoids, have been reported from *Trichilia* plants by different research groups (An et al., 2016; Cao et al., 2021; Ji et al., 2015; Liu et al., 2014; Solipeta et al., 2019; Wang et al., 2017). Given the diversity of limonoids in *Trichilia* species to date, we are encouraged to find more limonoids with different frameworks from this genus and explore their biological activities.

*Trichilia sinensis* Benth. (Meliaceae) is a shrub mainly distributed in Yunnan, Guangdong, and Guangxi provinces of China. As a kind of common traditional Chinese medicine, *T. sinensis* is used to treat abdominal pain, chronic osteomyelitis, scabies, eczema, rheumatism, and traumatic injury (Editorial Committee of Chinese Materia Medica, National Administration of Traditional Chinese Medicine, 1999). It was reported that *T. sinensis* afforded a series of highly rearranged limonoids,

\* Corresponding author. Key Laboratory of Research on Pathogenesis of Allergen Provoked Allergic Disease in Liaoning Province, Shenyang Medical College, Shenyang, 110034, China.

\*\* Corresponding author. State Key Laboratory of Medicinal Chemical Biology, College of Pharmacy, and Tianjin Key Laboratory of Molecular Drug Research, Nankai University, Tianjin, 300350, China.

E-mail addresses: [victgyq@nankai.edu.cn](mailto:victgyq@nankai.edu.cn) (Y. Guo), [huping1277@163.com](mailto:huping1277@163.com) (P. Hu).

<sup>1</sup> These authors contributed equally to this work.

<https://doi.org/10.1016/j.phytochem.2022.113502>

Received 17 June 2022; Received in revised form 31 October 2022; Accepted 3 November 2022

Available online 7 November 2022

0031-9422/© 2022 Elsevier Ltd. All rights reserved.

some of which were active against inflammation (Xu et al., 2013). Though many limonoids were obtained from *Trichilia* plants and several had anti-inflammatory activity, most of the activity investigations performed were limited to the cellular level. Considering the structural and biological diversity of limonoids in *T. sinensis* and the general lack of biological research on limonoids *in vivo*, such an examination of the chemical constituents on *T. sinensis* was conducted. As a result, four undescribed highly oxidized and rearranged limonoids (Fig. 1) were obtained from *T. sinensis*. The structures were determined by NMR, HRESIMS data analysis, and electronic circular dichroism (ECD) calculations. As undescribed examples of highly oxidized and rearranged limonoids, compound **1** was characterized as a rare 30-nortrijugin limonoid with an unusual cleavage of 1,14-ether linkage, **2** and **3** represented undescribed trijugin-type examples with the cleavage of  $\delta$ -lactone ring D, and **4** was a rare trijugin-type limonoid with an unusual 2,6-oxygen-bridge. Herein, we report the isolation, structural elucidation, NO inhibition via regulating inflammation-related protein expression, and anti-inflammatory effects of these limonoids *in vivo* obtained from *T. sinensis*.

## 2. Results and discussion

### 2.1. Previously undescribed limonoids 1–4

Secotrijugin A (**1**) was acquired as a colorless oil. The molecular formula was determined as  $C_{27}H_{32}O_{10}$  by the positive HRESIMS ion peak at  $m/z$  539.1890  $[M + Na]^+$  (calcd for  $C_{27}H_{32}O_{10}Na$ , 539.1893). The  $^1H$  NMR spectrum (Table 1) displayed signals assignable to five olefinic protons ( $\delta_H$  7.54, 7.43, 6.42, 6.80, and 5.78, each 1H, s), two oxymethine protons ( $\delta_H$  5.39 and 4.49, each 1H, s), four tertiary methyls ( $\delta_H$  1.57, 1.24, 1.08, and 1.04), as well as two methoxy groups ( $\delta_H$  3.83 and 3.78). The downfield olefinic proton signals ( $\delta_H$  7.54, 7.43, and 6.42), together with the diagnostic olefinic carbons ( $\delta_C$  121.1, 140.3, 108.9, and 143.2) occurring in the  $^{13}C$  and DEPT NMR spectra, discovered a typical  $\beta$ -substituted furan ring present in **1**. Excluding two methoxy carbons ( $\delta_C$  52.9 and 53.1) and four olefinic carbons belonging to the typical  $\beta$ -substituted furan ring, one ketone carbonyl ( $\delta_C$  201.8), three ester carbonyls ( $\delta_C$  176.6, 175.8, and 166.2), four extra olefinic carbons ( $\delta_C$  175.6, 111.0, 142.0, and 137.4) conjugated with carbonyls, three oxygenated carbons ( $\delta_C$  69.6, 80.5, and 82.3), and ten aliphatic carbons were observed from the  $^{13}C$  NMR spectrum (Table 1). The ten aliphatic carbons were distinguished as four methyls ( $\delta_C$  27.2, 26.3, 21.7, and 19.1), two methylenes ( $\delta_C$  39.1 and 34.1), one methine ( $\delta_C$  51.3), and three quaternary carbons ( $\delta_C$  46.0, 46.0, and 44.7). The above-mentioned NMR spectroscopic data implied compound **1** to be a limonoid (Wang et al., 2008; Zhang et al., 2003).

The  $^1H$ - $^1H$  COSY and HMBC experiments (Fig. 2) were conducted to analyze the exact structure of **1**. The HMBC correlations from H-17 to C-12, C-13, C-14, C-16, and C-18, H<sub>3</sub>-18 to C-12, C-13, C-14, and C-17, H-15 to C-8, C-13, and C-14, together with H<sub>2</sub>-11/H<sub>2</sub>-12 cross-peak in the  $^1H$ - $^1H$  COSY spectrum (Fig. 2), indicated a fused fragment composed of

an  $\alpha,\beta$ -unsaturated  $\delta$ -lactone ring D and a five-membered ring C with a methyl (CH<sub>3</sub>-18) connected to C-13, both of which shared the C-13–C-14 unit. Furthermore, another unsaturated six-membered ring A consisting of C-1–C-5 and C-10 was also inferred by the HMBC correlations from H<sub>3</sub>-19 to C-1, C-5, and C-10, H<sub>3</sub>-28/H<sub>3</sub>-29 to C-3, C-4, and C-5, and H-1 to C-2, C-3, C-5, and C-10. Besides bearing three methyls (CH<sub>3</sub>-19, CH<sub>3</sub>-28, and CH<sub>3</sub>-29) and a methoxycarbonyl group at C-10, C-4, C-4, and C-10, ring A was found to carry a 1-hydroxy-2-methoxy-2-oxoethyl group (C-6–C-7 unit) attached at C-5, which was demonstrated by the corresponding HMBC correlations of H-6 with C-4, C-5, C-7, and C-10, and the methoxy protons with C-7. The total four main fragments including rings A, C, D, and E were therefore defined by the above NMR data analysis. In addition to rings C and D sharing C-13–C-14 unit, the linkage of C-2 and C-8 between rings A and C and the fusion of rings D and E via C-17 and C-20 were disclosed and confirmed by the crucial HMBC correlations of H-1 with C-8, H<sub>2</sub>-11 with C-2, H-17 with C-20, C-21, and C-22, and H-21 (H-22) with C-17. Therefore, the planar structure of **1** was determined. The proton and carbon signals assignments were fulfilled via detailed analysis of the 1D and 2D NMR data.

The relative configuration of **1** was inferred by the Chem3D modeling and NOESY data. The NOESY interactions of H<sub>3</sub>-28/H-5, H-5/H-6, H<sub>3</sub>-29/H<sub>3</sub>-19, H<sub>3</sub>-19/H-1, H-1/H-12 $\beta$ , H<sub>3</sub>-18/H-12 $\alpha$ , and H-12 $\beta$ /H-17, together with Chem3D simulations, showed a steric configuration as shown in Fig. 3, in which H-5, H-6, CH<sub>3</sub>-18, and CH<sub>3</sub>-28 were  $\alpha$ -oriented, and H-17, CH<sub>3</sub>-19, and CH<sub>3</sub>-29 were  $\beta$ -oriented. The C-8 hydroxy group was inferred to be on the  $\alpha$ -side of ring C by the NOESY correlation of H-1/H-17 ( $\beta$ -orientation for H-17) and the biosynthetic pathway of limonoids (Wang et al., 2008; Zhang et al., 2003). The configuration of C-6 was inferred to be *rel*-6R by the coupling constant ( $J_{5,6} = \sim 0$  Hz) and the definitive NOESY correlations of H-6/H<sub>3</sub>-19 (Wang et al., 2008; Zhang et al., 2003). Furthermore, the final configuration of **1** was determined by TDDFT/ECD calculations (Liang et al., 2019). The calculated ECD spectrum showed identical Cotton effects with the experimental ECD data (Fig. 4A), resulting in the configurational assignment of chiral carbons being 5S, 6R, 8R, 10S, 13R, and 17R. Thus, the structure of **1** was characterized as shown in Fig. 1.

Secotrijugin B (**2**), a colorless oil, had a molecular ion peak at  $m/z$  597.2310  $[M + Na]^+$  (calcd for  $C_{30}H_{38}O_{11}Na$ , 597.2312) in the positive HRESIMS, corresponding to the molecular formula of  $C_{30}H_{38}O_{11}$ , which indicated twelve degrees of unsaturation. The  $^1H$  NMR and  $^{13}C$  NMR spectra (Table 1) showed the presence of one acetyloxy group ( $\delta_C$  169.0 and 20.0) and two methoxy groups ( $\delta_C$  51.8 and 51.9). In addition, the same  $\beta$ -substituted furan ring E as that of **1** was deduced from 1D NMR spectroscopic data ( $\delta_H$  7.68, 7.34, and 6.57;  $\delta_C$  126.1, 140.7, 109.9, and 142.5) of **2**. Besides these carbon signals for the above fragments, the  $^{13}C$  NMR spectrum, together with the DEPT spectrum, exhibited signals assignable to two ketone carbonyls ( $\delta_C$  212.9 and 206.1), two ester carbonyls ( $\delta_C$  173.5 and 171.6), two additional olefinic carbons ( $\delta_C$  143.9 and 116.2) forming a terminal double bond, and four oxygenated carbons ( $\delta_C$  75.6, 76.2, 89.6, and 67.1), as well as 12 aliphatic carbons [four methyls ( $\delta_C$  10.5, 18.4, 22.4, and 27.0), three methylenes ( $\delta_C$  41.4,

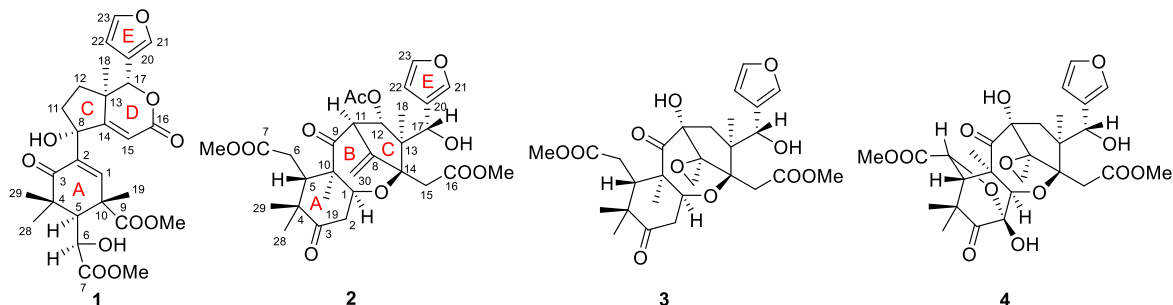


Fig. 1. Chemical structures of compounds 1–4.

**Table 1**  
 $^1\text{H}$  and  $^{13}\text{C}$  NMR data of compounds 1–4 in  $\text{CDCl}_3$  ( $\delta$  in ppm and  $J$  in Hz).

position	1		2		3		4	
	$\delta_{\text{H}}$	$\Delta\text{c}$	$\delta_{\text{H}}$	$\delta\text{c}$	$\delta_{\text{H}}$	$\delta\text{c}$	$\delta_{\text{H}}$	$\delta\text{c}$
1	6.80 s	142.0	4.69 dd (4.2, 2.8)		75.6	5.07 dd (3.7, 3.3)		74.6
2 $\alpha$		137.4	2.88 dd (16.4, 4.2)		41.4	3.01 dd (14.6, 3.3)		40.3
2 $\beta$			2.59 dd (16.4, 2.8)			2.84 dd (14.6, 3.7)		
3		201.8			212.9			211.7
4		44.7			49.0			49.3
5	3.39 s	51.3	3.27 dd (9.6, 1.9)		41.5	3.13 dd (5.6, 4.6)		43.5
6a	4.49 s	69.6	2.80 dd (17.6, 1.9)		30.5	2.81 dd (17.7, 5.6)		30.5
6 b			2.44 dd (17.6, 9.6)			2.45 dd (17.7, 4.6)		
7		175.8			173.5			173.4
8		80.5			143.9			68.0
9		176.6			206.1			211.7
10		46.0			55.8			54.4
11 $\alpha$	2.11 m	39.1	3.21 d (2.7)		68.5			81.5
11 $\beta$	2.19 m							
12 $\alpha$	1.73 m	34.1			76.2	1.25 d (15.0)		46.8
12 $\beta$	2.14 m		5.10 d (2.7)			2.97 d (15.0)		2.31 d (15.1)
13		46.0			56.2			51.0
14		175.6			89.6			84.8
15a	5.78 s	111.0	3.77 d (15.6)		36.0	3.16 d (14.3)		35.2
15 b			2.87 d (15.6)			2.51 d (14.3)		2.63 d (15.5)
16		166.2			171.6			171.2
17	5.39 s	82.3	5.47 s		67.1	5.20 s		67.5
18	1.24 s	19.1	1.01 s		10.5	1.17 s		17.3
19	1.57 s	26.3	1.11 s		18.4	1.33 s		18.3
20		121.1			126.1			125.9
21	7.54 s	140.3	7.68 s		140.7	7.48 s		140.3
22	6.42 s	108.9	6.57 s		109.9	6.50 s		110.0
23	7.43 s	143.2	7.34 s		142.5	7.36 s		142.6
28	1.08 s	27.2	1.15 s		22.4	1.17 s		22.6
29	1.04 s	21.7	1.20 s		27.0	1.13 s		25.1
30a			5.46 s		116.2	3.12 d (5.3)		46.9
30 b			5.36 s			2.83 d (5.3)		2.77 s
OMe-7	3.83 s	52.9	3.70 s		51.8	3.63 s		52.0
OMe-9	3.78 s	53.1						3.78 s
OMe-16			3.74 s		51.9	3.74 s		52.1
OAc-12			1.63 s		20.0			3.72 s
					169.0			

36.0, and 30.5), two methines ( $\delta\text{c}$  68.5 and 41.5), and three quaternary carbons ( $\delta\text{c}$  56.2, 55.8, and 49.0)]. These typically spectroscopic features, especially the total 26 skeletal carbons and the  $\beta$ -substituted furan ring, indicated that compound **2** possessed a polycyclic trijugin-type limonoid scaffold as shown in Fig. 1, according to the comparison of its  $^{13}\text{C}$  NMR data with those of known compounds (An et al., 2018; Di et al., 2007). This distinctive skeleton of a trijugin-type limonoid was verified by  $^1\text{H}$ - $^1\text{H}$  COSY and HMBC (Fig. 2) experiments. Combinational analysis of the NMR data of **2**, particularly the HMBC data, led to the construction of the planar structure of **2**, which comprised rings A, B, C, and E and two 2-methoxy-2-oxoethyl groups ( $-\text{CH}_2\text{COOCH}_3$ , C-6–C-7 unit and C-15–C-16 unit). Correspondingly, the skeletal ketone and ester carbonyls [ $\delta\text{c}$  212.9 (C-3), 206.1 (C-9), 173.5 (C-7), and 171.6 (C-16)], olefinic carbons [ $\delta\text{c}$  143.9 (C-8), 126.1 (C-20), 140.7 (C-21), 109.9 (C-22), 142.5 (C-23), and 116.2 (C-30)], and oxygenated carbons [ $\delta\text{c}$  75.6 (C-1), 76.2 (C-12), 89.6 (C-14), and 67.1 (C-17)], and also the other skeletal proton and carbon signals, were assigned. The residual substituent group (acetyloxy group) was demonstrated to be attached at C-12 based on the HMBC correlation of H-12 to the carbonyl of the acetyloxy moiety. The planar structure of **2** was thus established (Fig. 2), which was very similar to that of 12-acetyloxytrijugin B (Yang et al., 2021) and only differed from that by the cleavage of  $\delta$ -lactone ring D to form 16-methyl ester and 17-hydroxy.

The steric configuration of **2** was inferred by Chem3D modeling and the NOESY spectrum (Fig. 3). The NOESY spectrum showed vital correlations of H<sub>3</sub>-29/H-5, H-5/H-12, H-12/H-17, H<sub>3</sub>-19/H-1, H-30b/H-11, H-30a/H-15 b, and H<sub>3</sub>-18/H-15 b. According to these NOE correlations, H<sub>3</sub>-29, H-5, and H-12 were on the same side and assigned being  $\beta$ -orientations, and H<sub>3</sub>-28, H<sub>3</sub>-19, H-1, H-11, H<sub>3</sub>-18, and C-30 were assigned

as  $\alpha$ -orientations. It's difficult to judge the configuration of C-17 due to the cleavage of  $\delta$ -lactone ring D. However, it should be noted that the cleavage of  $\delta$ -lactone ring D was only the ester hydrolysis, which did not affect the configuration of C-17 (Zhang et al., 2003). So, the C-17 configuration was presumed to be *rel*-17S. The ECD calculations of **2** were performed, and the resulting calculated ECD spectrum matched experimental ECD spectrum well (Fig. 4B), allowing the absolute configuration of **2** to be defined as 1S, 5S, 10R, 11R, 12S, 13R, 14S, and 17S. Thus, the final structure of **2** was established as shown in Fig. 1.

Secotrijugin C (**3**) was acquired as a colorless oil. The HRESIMS disclosed a sodium adduct ion at  $m/z$  571.2152 [ $\text{M} + \text{Na}$ ]<sup>+</sup> (calcd for C<sub>28</sub>H<sub>36</sub>O<sub>11</sub>Na, 571.2155), implying a molecular formula of C<sub>28</sub>H<sub>36</sub>O<sub>11</sub>. The  $^1\text{H}$  and  $^{13}\text{C}$  NMR spectra (Table 1) had high similarities with those of compound **2**, which indicated that compound **3** was also a trijugin-type limonoid closely similar to **2** structurally. Following the comparison of their  $^1\text{H}$  and  $^{13}\text{C}$  NMR spectra, it could be shown that the acetyloxy group in **3** was absent and the  $\Delta^{8,30}$  double bond in **2** was oxidized to form 8,30-epoxy group in **3** by the chemical shifts of C-8 ( $\delta\text{c}$  68.0) and C-30 ( $\delta\text{c}$  46.9). To corroborate these inferences, a series of NMR experiments including DEPT,  $^1\text{H}$ - $^1\text{H}$  COSY, HMQC, and HMBC were carried out. The following deduction about the  $^1\text{H}$ - $^1\text{H}$  COSY, HMQC, and HMBC data led to the construction of rings A, B, C, and E, 8,30-epoxy moiety, and two 2-methoxy-2-oxoethyl groups ( $-\text{CH}_2\text{COOCH}_3$ , C-6–C-7 unit and C-15–C-16 unit), which were fused or linked to constitute a structure for **3** as shown in Fig. 2. The planar structure of **3** was established, which differed from compound **2** by the formation of 8,30-epoxy moiety and the shift of oxygenated carbon from C-12 to C-11.

The NOESY data disclosed that the gross molecular conformation of **3** resembled that of compound **2** (Fig. 3). In this conformation, the

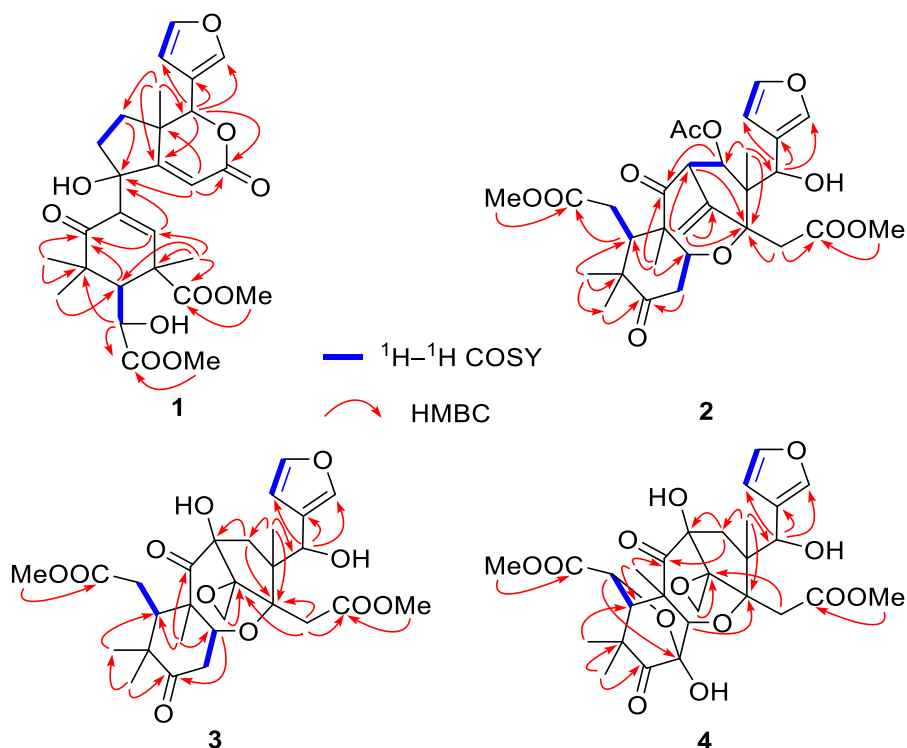


Fig. 2.  $^1\text{H}$ - $^1\text{H}$  COSY and key HMBC correlations of 1-4.

configuration of C-8 in **3** was assigned as *rel*-8S by the NOESY correlations of H-30 b/H<sub>3</sub>-18, and the C-11 hydroxy should adopt an  $\alpha$ -orientation according to the conformations of rings B and C and the biosynthesis pathway of trijugin-type limonoids (An et al., 2018; Di et al., 2007). By comparing the Cotton effects in the calculated and experimental ECD curves (Fig. 4C), the absolute configuration of **3** was deduced as 1S, 5S, 8S, 10R, 11R, 13S, 14R, and 17S. The structure of **3** was finally characterized as shown in Fig. 1.

Secotrijugin D (**4**), a colorless oil, possessed a molecular formula of C<sub>28</sub>H<sub>34</sub>O<sub>13</sub> according to the HRESIMS ( $m/z$  601.1895 [M + Na]<sup>+</sup>, calcd for C<sub>28</sub>H<sub>34</sub>O<sub>13</sub>Na, 601.1897) and the <sup>13</sup>C NMR data analysis. The molecular formula indicated twelve degrees of unsaturation. The <sup>1</sup>H and <sup>13</sup>C NMR spectra (Table 1) of **4** resembled those of **3**, suggesting **4** to be also a trijugin-type limonoid structurally related to compound **3**. The subsequent 2D NMR experiments and data analysis disclosed the presence of rings B, C, and E, 8,30-epoxy moiety, and the cleaved  $\delta$ -lactone ring D to form 16-methyl ester and 17-hydroxy, which were the same as those present in **3**. In addition, comparison the 1D NMR data (Table 1) of **4** with **3** indicated that two of the methylenes in **3** were replaced by an acetal carbon ( $\delta_{\text{C}}$  95.0) and an oxymethine in **4**. All the above NMR data analysis pointed out that the difference between the two compounds lied in ring A. The subsequent analysis of 1D and 2D NMR data enabled the ring A bearing the C-6-C-7 unit and three methyls (CH<sub>3</sub>-28, CH<sub>3</sub>-29, and CH<sub>3</sub>-19) to be elucidated, where the aforementioned acetal and oxymethine carbon signals at  $\delta_{\text{C}}$  95.0 and  $\delta_{\text{C}}$  72.8 were assigned to C-2 and C-6, respectively. The overall planar structure of **4** seemed to be established. However, this structure deduced from the NMR data for **4** was inconsistent with the HRESIMS data by 18 more mass unit and one less index of hydrogen insufficiency, which implied one more ring present in **4**. Reinvestigation of the HMBC data (Fig. 2) disclosed the long-range correlation of H-6 ( $\delta_{\text{H}}$  4.97) to the acetal carbon C-2 ( $\delta_{\text{C}}$  95.0), a 2,6-epoxy moiety was thus proposed, and the planar structure of **4** was elucidated by the above NMR and HRESIMS data analysis.

A NOESY experiment was conducted to establish the relative configuration of **4**. According to the NOESY interactions observed from

the NOESY spectrum, together with the Chem3D simulations (Fig. 3), a general molecular conformation for **4** was proposed and depicted in Fig. 3, which was similar to that of **3** except for ring A. From this steric conformation of **4**, ring A presented a boat conformation due to the 2,6-epoxy moiety that existed on the  $\alpha$ -face of ring A. The C-6 configuration was determined *rel*-6R by the NOESY correlation of H-6/H<sub>3</sub>-19. The ECD calculations provided the calculated ECD spectrum of **4**. The analogical Cotton effects in the calculated and experimental ECD spectra (Fig. 4D), allowed the absolute configuration of **4** to be deduced as 1R, 2S, 5S, 6R, 8S, 10R, 11R, 13S, 14R, and 17S. Thus, the ultimate structure of **4** was established as shown in Fig. 1.

## 2.2. Nitric oxide (NO) inhibitory assay of the isolated compounds

NO, as an inflammatory mediator in inflammatory diseases, is an important signal molecule in many physiological and biochemical processes. Therefore, inhibition of NO production may control the development of inflammation. Limonoids, as a unique class of natural products, not only possess diverse chemical structures, but also have various biological characteristics. To explore the potential medicinal applications for anti-inflammatory drug development, these limonoids isolated from *T. sinensis* were assessed for their inhibitory effects on LPS-stimulated NO production in BV-2 cells. The SMT (2-methyl-2-thio-pseudourea, sulfate) was used as the positive control (IC<sub>50</sub> value of 4.5  $\mu\text{M}$ ). According to screening results, compound **2** had prominent NO inhibitory activity with IC<sub>50</sub> value of 16.7  $\mu\text{M}$ , compound **3** had moderate inhibitory effects (IC<sub>50</sub> value of 46.7  $\mu\text{M}$ ), and **1** and **4** were almost inactive (IC<sub>50</sub> > 100  $\mu\text{M}$ ). At the effective concentration, the tested compounds did not show obvious cytotoxicity to BV-2 cells.

## 2.3. Assessment of COX-2 and iNOS activity

During inflammation, the inflammatory signaling pathway is activated, and the corresponding proteins, such as COX-2 and iNOS are highly expressed, resulting in the release of excessive NO production.

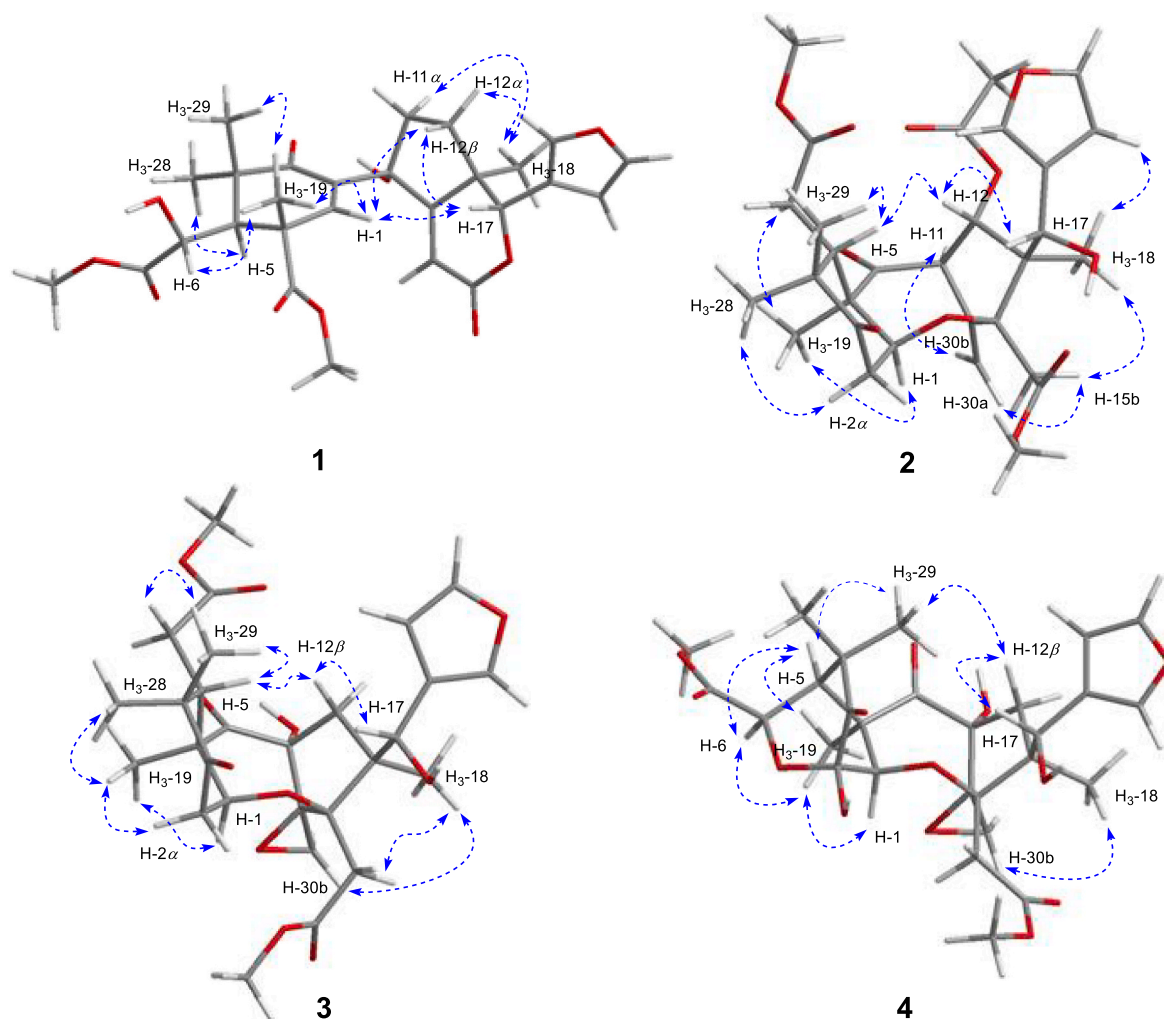


Fig. 3. Conformations and key NOESY correlations of 1–4.

Compound 2 was found to be the most active against NO production in LPS-induced BV-2 cells. To understand the possible anti-inflammatory mechanism of the active compounds, the LPS-induced BV-2 cells were treated with 2 and the protein expression of COX-2 and iNOS was detected by Western blotting experiments. As shown in Fig. 5, LPS stimulation prompted the expression of COX-2 and iNOS evidently. After being treated with compound 2, COX-2 and iNOS were inhibited dose-dependently, which suggested that the anti-inflammatory effects of 2 was accomplished by downregulating COX-2 and iNOS protein expression.

#### 2.4. *In vivo* anti-inflammatory assessment of compound 2

The possible anti-inflammatory application of compound 2 was further discussed using an *in vivo* model. Considering the limited amount of natural products obtained, zebrafish was selected to establish an *in vivo* screening model, which is a convenient and economical animal screening model and very suitable for *in vivo* screening of natural products (Shi et al., 2020). Using the established zebrafish model, in addition to detecting excessive NO, ROS production in zebrafish was also detected, which is also one of the indicators of inflammatory response. As illustrated in Figs. 6 and 7, LPS induced the increase of ROS and NO production significantly in zebrafish model. The levels of ROS and NO decreased dose-dependently after administration of 2, which indicated that compound 2 inhibited ROS and NO generation and had strong anti-inflammatory effects *in vivo*.

### 3. Conclusions

In the present study, four previously undescribed trijugin-type limonoids (1–4) were characterized from the twigs and leaves of *T. sinensis*. Compound 1 was found to possess a rare 30-nortrijugin-type framework via the further degradation of trijugin-type limonoids. The first 30-nortrijugin-type limonoid and its possible biosynthesis pathway were reported in 2003 (Zhang et al., 2003), and the total number of 30-nortrijugin-type limonoids reported is less than 10 so far. Compound 4 was characterized as a unique trijugin-type limonoid with the presence of an unusual 2,6-oxygen bridge, and the similar trijugin-type limonoids containing 2,6-oxygen bridge have been rarely reported. All of the trijugin-type limonoids were evaluated and compound 2 was the most active against NO production in LPS-induced BV-2 cells, which exerted anti-inflammatory effects by downregulating COX-2 and iNOS protein expression. The further zebrafish experiments confirmed that 2 had strong *in vivo* anti-inflammatory activity via suppressing ROS and NO generation. All of the biological results suggested that the most active compound 2 is potentially useful in the discovery of anti-inflammatory lead compound.

### 4. Experimental

#### 4.1. General

An InsMark IP120 automatic polarimeter was used to measure

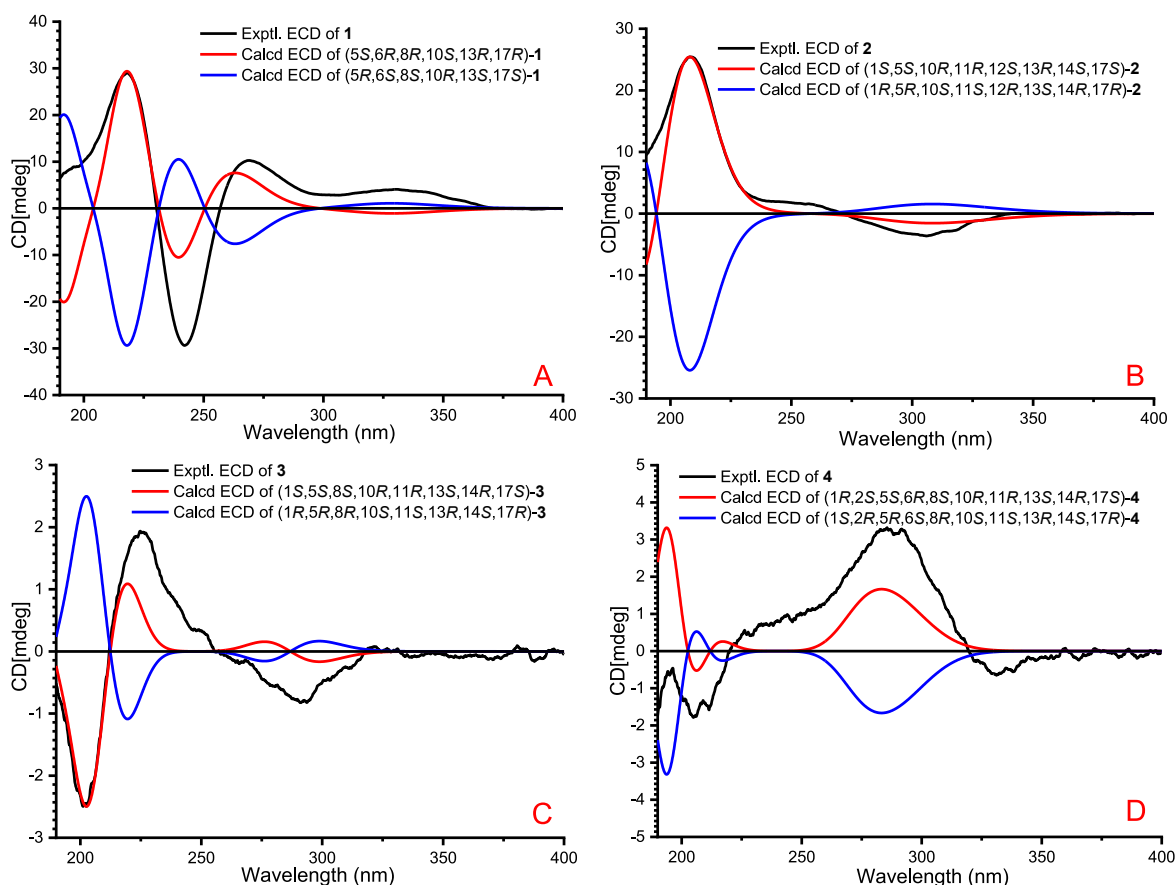


Fig. 4. Calculated and experimental ECD spectra of 1–4 (A–D) in acetonitrile.

optical rotations. The JASCO J-715 CD spectrometer was used to get the ECD spectra. Infrared (IR) spectra were measured by Bruker Tensor 37 FT-IR spectrometer (KBr disks). NMR spectra were obtained on a Bruker AV 400 instrument. An IonSpec 7.0 T FTICR MS was used to get the HRESIMS data. Silica gel was provided by Qingdao Haiyang Chemical Group Co., Ltd. Chemical reagents (analytical grade) were provided by Tianjin Chemical Reagent Co. and biological reagents were provided by Sigma Co.

#### 4.2. Plant material

The twigs and leaves of *Trichilia sinensis* Benth. (Meliaceae) were gathered from Yunnan province (E 99°56', N 21°08') of China in October 2017. The plant was identified by Yuanqiang Guo. The laboratory of Natural Medicinal Chemistry of Nankai University has preserved the voucher specimen (No. 20171015).

#### 4.3. Extraction and isolation

The twigs and leaves of *T. sinensis* (4.5 kg) were extracted three times with MeOH (3 × 36 L). The solution obtained was concentrated *in vacuo* to give a crude extract (985.0 g). Then, the residue was dissolved in water and partitioned with ethyl acetate to afford the EA-soluble portion (354.0 g). The portion was fractionated by silica gel column eluted with a gradient solvent system of petroleum ether-acetone to give eight fractions (A–H). Fraction H was then purified by ODS column eluted with MeOH–H<sub>2</sub>O (from 60 to 90%, v/v) to give eight subfractions H1–H8. Fraction H5 was fractionated with preparative HPLC to give compound 1 (*t<sub>R</sub>* = 25 min, 9.8 mg) using 70% MeOH in H<sub>2</sub>O as eluent. Similarly, compound 4 (*t<sub>R</sub>* = 26 min, 8.2 mg) was gained from sub-fraction H1 by preparative HPLC eluted with 62% MeOH–H<sub>2</sub>O. Using

the same procedure as fraction H, Fraction E gave seven subfractions E1–E7. The subsequent purification of E2 by preparative HPLC system (77% MeOH in H<sub>2</sub>O) gave compound 2 (*t<sub>R</sub>* = 21 min, 9.5 mg). Using the same MPLC, fraction F gave eight subfractions F1–F8. Compound 3 (*t<sub>R</sub>* = 32 min, 9.2 mg) was acquired from F2 by preparative HPLC (69% MeOH–H<sub>2</sub>O).

*Secotrijugin A (1)* colorless oil;  $[\alpha]_D^{14} +28$  (c 0.3, MeOH); ECD (CH<sub>3</sub>CN) 218 ( $\Delta\epsilon +9.08$ ), 242 ( $\Delta\epsilon -9.20$ ), 269 ( $\Delta\epsilon +3.22$ ) nm; IR (KBr)  $\nu_{\max}$  3446, 2934, 1733, 1684, 1457, 1234, 1158, 1123, 1025, 876, 736, 602 cm<sup>-1</sup>; <sup>13</sup>C NMR (100 MHz, CDCl<sub>3</sub>) and <sup>1</sup>H NMR (400 MHz, CDCl<sub>3</sub>) data, see Table 1; ESIMS *m/z* 539 [M + Na]<sup>+</sup>; HRESIMS *m/z* 539.1890 [M + Na]<sup>+</sup>, calcd for C<sub>27</sub>H<sub>32</sub>O<sub>10</sub>Na, 539.1893.

*Secotrijugin B (2)* colorless oil;  $[\alpha]_D^{14} -11$  (c 0.3, MeOH); ECD (CH<sub>3</sub>CN) 209 ( $\Delta\epsilon +8.86$ ) nm; IR (KBr)  $\nu_{\max}$  3447, 2951, 1735, 1437, 1374, 1236, 1051, 1030, 735 cm<sup>-1</sup>; <sup>13</sup>C NMR (100 MHz, CDCl<sub>3</sub>) and <sup>1</sup>H NMR (400 MHz, CDCl<sub>3</sub>) data, see Table 1; ESIMS *m/z* 597 [M + Na]<sup>+</sup>; HRESIMS *m/z* 597.2310 [M + Na]<sup>+</sup>, calcd for C<sub>30</sub>H<sub>38</sub>O<sub>11</sub>Na, 597.2312.

*Secotrijugin C (3)* colorless oil;  $[\alpha]_D^{14} -16$  (c 0.3, MeOH); ECD (CH<sub>3</sub>CN) 203 ( $\Delta\epsilon -0.83$ ), 225 ( $\Delta\epsilon +0.64$ ) nm; IR (KBr)  $\nu_{\max}$  3446, 2952, 1734, 1718, 1686, 1437, 1386, 1263, 1200, 1177, 1073, 1027, 875, 736, 602 cm<sup>-1</sup>; <sup>13</sup>C NMR (100 MHz, CDCl<sub>3</sub>) and <sup>1</sup>H NMR (400 MHz, CDCl<sub>3</sub>) data, see Table 1; ESIMS *m/z* 571 [M + Na]<sup>+</sup>; HRESIMS *m/z* 571.2152 [M + Na]<sup>+</sup>, calcd for C<sub>28</sub>H<sub>36</sub>O<sub>11</sub>Na, 571.2155.

*Secotrijugin D (4)* colorless oil;  $[\alpha]_D^{14} -7$  (c 0.3, MeOH); ECD (CH<sub>3</sub>CN) 205 ( $\Delta\epsilon -1.25$ ), 286 ( $\Delta\epsilon +2.33$ ) nm; IR (KBr)  $\nu_{\max}$  3446, 2953, 1733, 1717, 1438, 1232, 1166, 1071, 1028, 875, 735, 602 cm<sup>-1</sup>; <sup>13</sup>C NMR (100 MHz, CDCl<sub>3</sub>) and <sup>1</sup>H NMR (400 MHz, CDCl<sub>3</sub>) data, see Table 1; ESIMS *m/z* 601 [M + Na]<sup>+</sup>; HRESIMS *m/z* 601.1895 [M + Na]<sup>+</sup>, calcd for C<sub>28</sub>H<sub>34</sub>O<sub>13</sub>Na, 601.1897.

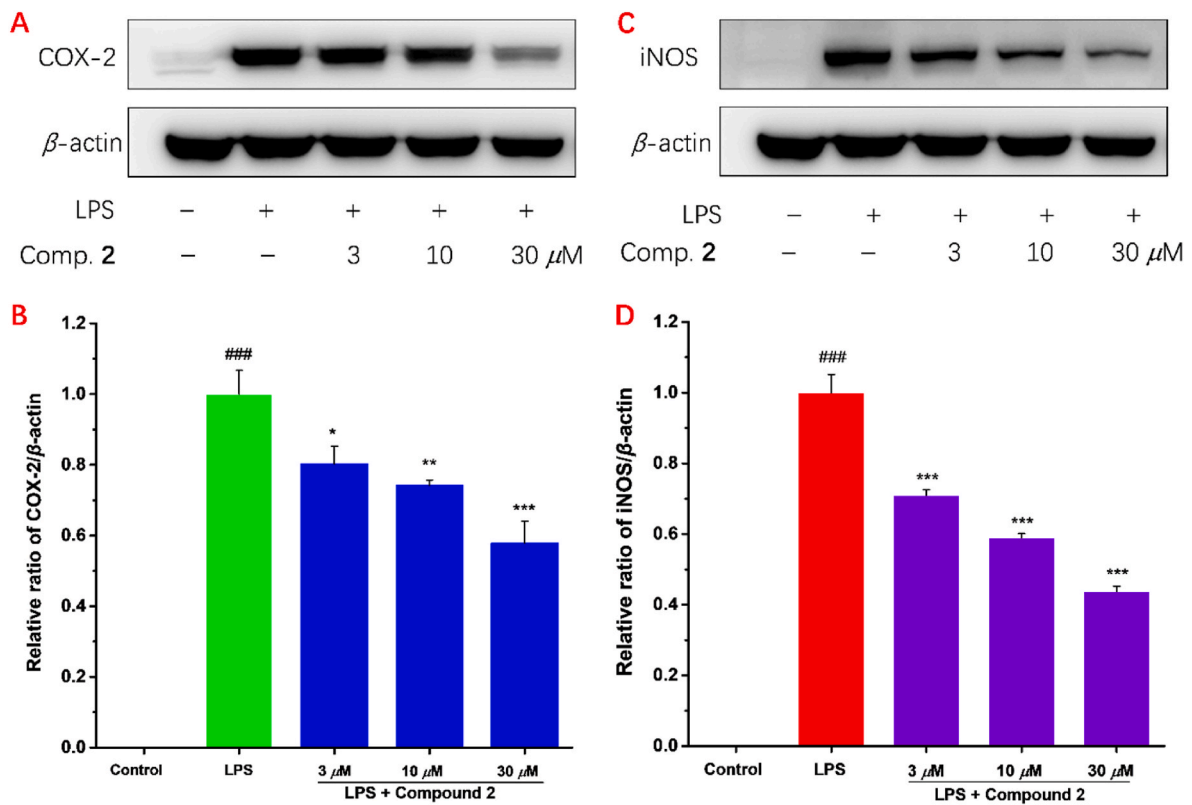


**Fig. 5.** Effects of 2 on iNOS and COX-2 expression in LPS-induced BV-2 cells. BV-2 cells were pretreated with 2 with 10, 30, and 100 μM for 30 min and then stimulated with LPS for 24 h, cells were harvested, and total protein was extracted. Protein band intensity was normalized to β-actin and was expressed as fold difference relative to the LPS group (down). <sup>###</sup>*p* < 0.001, compared with control, <sup>\*\*\*</sup>*p* < 0.001; <sup>\*\*</sup>*p* < 0.01, <sup>\*</sup>*p* < 0.05, compared with LPS group.

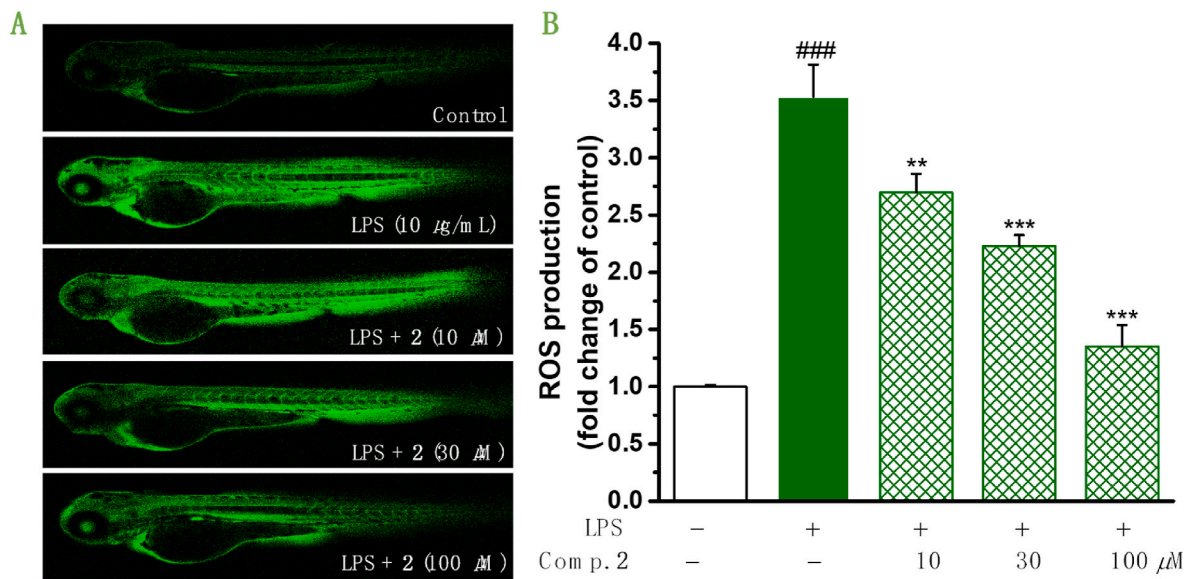


**Fig. 6.** Effects of 2 on ROS production in LPS-stimulated zebrafish embryos. Zebrafish embryos were induced by LPS (10 μg/ml) and given with or without 2 (10, 30, and 100 μM) for 24 h. At 3 day post fertilization (dpf), the ROS levels were detected and observed by laser confocal microscope. Fluorescence intensity was quantified using Image J. Data were expressed as mean ± SD. <sup>###</sup>*p* < 0.001 compared with LPS-untreated embryos, <sup>\*\*\*</sup>*p* < 0.001, <sup>\*\*</sup>*p* < 0.01 compared with LPS-treated group.

4.4. ECD calculations

The ECD calculations were conducted by the method reported previously (Frisch et al., 2013).

4.5. Cell survival assay, bioassay for NO production, and western blotting

Cell survival assay, the evaluation for NO inhibition, and Western blotting experiments were performed as previously reported (Du et al., 2020; Liang et al., 2019; Xu et al., 2016).

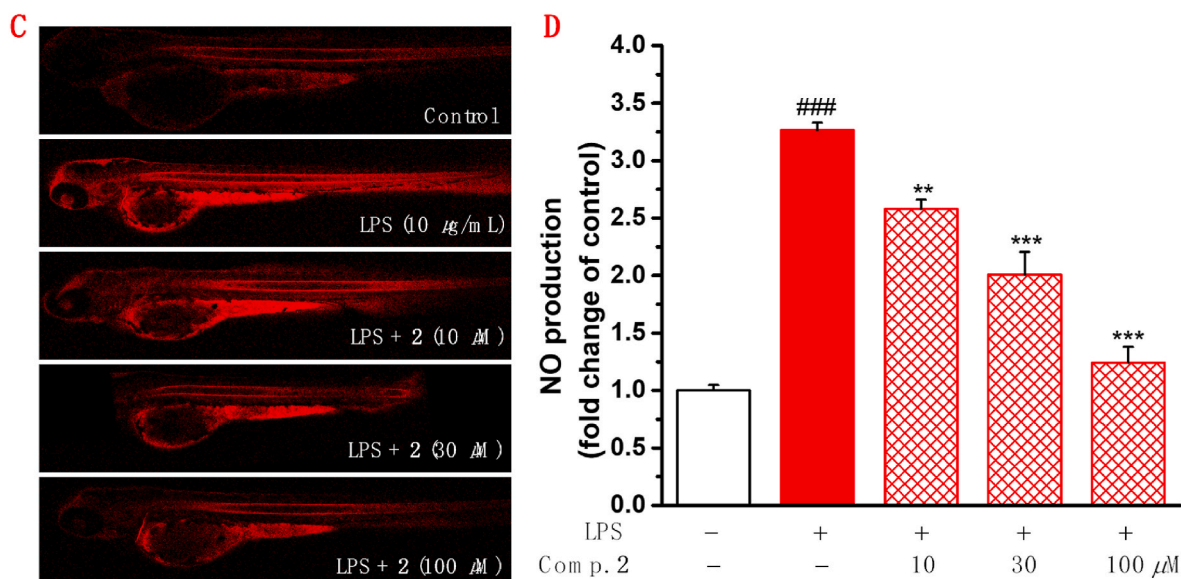


**Fig. 7.** Effects of 2 on NO production in LPS-stimulated zebrafish embryos. Zebrafish embryos were stimulated by LPS (10 µg/ml) with or without 2 (10, 30, and 100 µM) for 24 h. At 3 day post fertilization (dpf), the NO levels were measured by laser confocal microscope. Fluorescence intensity was quantified using Image J. Data were expressed as mean ± SD. ###*p* < 0.001 compared with LPS-untreated embryos, \*\*\**p* < 0.001, \*\**p* < 0.05 compared with LPS-treated group.

#### 4.6. Detection of NO and ROS in zebrafish model

The generation of ROS and NO in the zebrafish embryos was evaluated by DCFH-DA fluorescent probe dye and DAF-FMDA fluorescent probe dye, respectively (Wu et al., 2020). Zebrafish husbandry and embryo collection were conducted based on the methods reported (Wu et al., 2020). The experimental details are provided in the Supporting Information.

#### Declaration of competing interest

The authors declare that they have no known competing financial interests or personal relationships that could have appeared to influence the work reported in this paper.

#### Data availability

No data was used for the research described in the article.

#### Acknowledgements

This research was supported financially by the National Natural Science Foundation of China (Nos. 22177054 and U1801288), and the Natural Science Foundation of Liaoning Province, China (No. LJKZ1143).

#### Appendix A. Supplementary data

Supplementary data to this article can be found online at <https://doi.org/10.1016/j.phytochem.2022.113502>.

#### References

- An, F.L., Luo, J., Li, R.J., Luo, J.G., Wang, X.B., Yang, M.H., Yang, L., Yao, H.Q., Sun, H. B., Chen, Y.J., Kong, L.Y., 2016. Spirotrichilins A and B: two rearranged spirocyclic limonoids from *Trichilia connaroides*. *Org. Lett.* 18, 1924–1927. <https://doi.org/10.1021/acs.orglett.6b00738>.
- An, F.L., Sun, D.M., Wang, R.Z., Yang, M.H., Luo, J., Kong, L.Y., 2018. Trijugin- and mexicanolide-type limonoids from the fruits of *Heynea trijuga* that reverse multidrug resistance in MCF-7/DOX cells. *Phytochemistry* 151, 42–49. <https://doi.org/10.1016/j.phytochem.2018.04.004>.

- Cao, D.H., Yao, J.N., Sun, P., Ji, K.L., Li, X.N., Cai, Q., Xiao, C.F., Hu, H.B., Yu, Z.Y., Xu, Y.K., 2021. Structurally diverse limonoids and bio-active evaluation from *Trichilia connaroides*. *Fitoterapia* 153, 105001. <https://doi.org/10.1016/j.fitote.2021.105001>.
- Di, Y.T., He, H.P., Liu, H.Y., Yi, P., Zhang, Z., Ren, Y.L., Wang, J.S., Sun, Q.Y., Yang, F.M., Fang, X., Li, S.L., Zhu, H.J., Hao, X.J., 2007. Trijugin-type limonoids from the leaves of *Cipadessa cinerascens*. *J. Nat. Prod.* 70, 1352–1355. <https://doi.org/10.1021/np0700624>.
- Du, M., An, L.J., Xu, J., Guo, Y., 2020. Euphnerins A and B, diterpenoids with a 5/6/6 rearranged spirocyclic carbon skeleton from the stems of *Euphorbia nerifolia*. *J. Nat. Prod.* 83, 2592–2596. <https://doi.org/10.1021/acs.jnatprod.0c00249>.
- Editorial Committee of Chinese Materia Medica, National Administration of Traditional Chinese Medicine, 1999. *Chinese Materia Medica* (Zhonghua Bencao), 13. Shanghai Science & Technology Press, Shanghai, pp. 48–49.
- Editorial Committee of the Flora of China, Chinese Academy of Sciences, 1997. *Flora of China*, 43(3). Science Press, Beijing, p. 68.
- Frisch, M.J., Trucks, G.W., Schlegel, H.B., Scuseria, G.E., Robb, M.A., Cheeseman, J.R., et al., 2013. Gaussian 09, Revision D.01. Gaussian Inc, Wallingford, CT.
- Ji, K.L., Zhang, P., Li, X.N., Guo, J., Hu, H.B., Xiao, C.F., Xie, X.Q., Xu, Y.K., 2015. Cytotoxic limonoids from *Trichilia americana* leaves. *Phytochemistry* 118, 61–67. <https://doi.org/10.1016/j.phytochem.2015.08.014>.
- Li, W.S., Mándi, A., Liu, J.J., Shen, L., Kurtán, T., Wu, J., 2019. Xylomolones A–D from the Thai mangrove *Xylocarpus moluccensis*: assignment of absolute stereostructures and unveiling a convergent strategy for limonoid biosynthesis. *J. Org. Chem.* 84, 2596–2606. <https://doi.org/10.1021/acs.joc.8b03037>.
- Li, W.S., Wu, J., Li, J., Satyanandamurthy, T., Shen, L., Bringmann, G., 2017. Krishnadimer A, an axially chiral non-biaryl natural product: discovery and biomimetic synthesis. *Org. Lett.* 19, 182–185. <https://doi.org/10.1021/acs.orglett.6b03479>.
- Liang, Y., An, L., Shi, Z., Zhang, X., Xie, C., Tuerhong, M., Song, Z., Ohizumi, Y., Lee, D., Shuai, L., Xu, J., Guo, Y., 2019. Bioactive diterpenoids from the stems of *Euphorbia antiquorum*. *J. Nat. Prod.* 82, 1634–1644. <https://doi.org/10.1021/acs.jnatprod.9b00134>.
- Liu, C.P., Wang, G.C., Gan, L.S., Xu, C.H., Liu, Q.F., Ding, J., Yue, J.M., 2016. Ciliatonoids A and B, two limonoids from *Toona ciliata*. *Org. Lett.* 18, 2894–2897. <https://doi.org/10.1021/acs.orglett.6b01213>.
- Liu, C.P., Xu, J.B., Han, Y.S., Wainberg, M.A., Yue, J.M., 2014. Trichiconins A–C, limonoids with new carbon skeletons from *Trichilia connaroides*. *Org. Lett.* 16, 5478–5481. <https://doi.org/10.1021/ol5027552>.
- Lv, C., Yan, X., Tu, Q., Di, Y., Yuan, C., Fang, X., Ben-David, Y., Xia, L., Gong, J., Shen, Y., Yang, Z., Hao, X., 2016. Isolation and asymmetric total synthesis of Perforanoid A. *Angew. Chem.* 128, 7665–7669. <https://doi.org/10.1002/anie.201602783>.
- Shi, Z., An, L., Zhang, S., Li, Z., Li, Y., Cui, J., Zhang, J., Jin, D.Q., Tuerhong, M., Abudukeremu, M., Xu, J., Guo, Y., 2020. A heteropolysaccharide purified from leaves of *Ilex latifolia* displaying immunomodulatory activity *in vitro* and *in vivo*. *Carbohydr. Polym.* 245, 116469. <https://doi.org/10.1016/j.carbpol.2020.116469>.
- Solipeta, D.R., Bandi, S., Vemulapalli, S.P.B., Pallavi, P.M.C., Vemireddy, S., Balasubramania, S., Mahabalarao, S.K.H., Katragadda, S.B., 2019. Secopragmalin-type limonoids from *Trichilia connaroides*: isolation, semisynthesis, and their cytotoxic activities. *J. Nat. Prod.* 82, 2731–2743. <https://doi.org/10.1021/acs.jnatprod.9b00346>.



- Sun, Y.J., Cui, L.T., Sun, Y.P., Li, Q.R., Li, Y.Y., Wang, Z.F., Xu, W.J., Kong, L.Y., Luo, J., 2022. A/D-rings-*seco* limonoids from the fruits of *Aglaia edulis* and their bioactivities. *Phytochemistry* 195, 113049. <https://doi.org/10.1016/j.phytochem.2021.113049>.
- Tan, Q.G., Luo, X.D., 2011. Meliaceous limonoids: chemistry and biological activities. *Chem. Rev.* 111, 7437–7522. <https://doi.org/10.1021/cr9004023>.
- Tsakamoto, Y., Oya, H., Kikuchi, T., Yamada, T., Tanaka, R., 2019. Guianofruits C–I from fruit oil of andiroba (*Carapa guianensis*, Meliaceae). *Tetrahedron* 75, 1149–1156. <https://doi.org/10.1016/j.tet.2018.12.036>.
- Wang, G.C., Fan, Y.Y., Shyaula, S.L., Yue, J.M., 2017. Triconoids A–D, four limonoids possess two rearranged carbon skeletons from *Trichilia connaroides*. *Org. Lett.* 19, 2182–2185. <https://doi.org/10.1021/acs.orglett.7b00873>.
- Wang, X.N., Fan, C.Q., Yin, S., Gan, L.S., Yue, J.M., 2008. Structural elucidation of limonoids and steroids from *Trichilia connaroides*. *Phytochemistry* 69, 1319–1327. <https://doi.org/10.1016/j.phytochem.2008.01.018>.
- Wu, P., Song, Z., Li, Y., Wang, H., Zhang, H., Bao, J., Li, Y., Cui, J., Jin, D.Q., Wang, A., Liang, B., Lee, D., Xu, J., Guo, Y., 2020. Natural iridoids from *Patrinia heterophylla* showing anti-inflammatory activities *in vitro* and *in vivo*. *Bioorg. Chem.* 104, 104331. <https://doi.org/10.1016/j.bioorg.2020.104331>.
- Xu, J.B., Lin, Y., Dong, S.H., Wang, F., Yue, J.M., 2013. Trichinenlides A–T, mexicanolide-type limonoids from *Trichilia sinensis*. *J. Nat. Prod.* 76, 1872–1880. <https://doi.org/10.1021/np400408s>.
- Xu, J., Wang, M., Sun, X., Ren, Q., Cao, X., Li, S., Su, G., Tuerhong, M., Lee, D., Ohizumi, Y., Bartlam, M., Guo, Y., 2016. Bioactive terpenoids from *Salvia plebeia*: structures, NO inhibitory activities, and interactions with iNOS. *J. Nat. Prod.* 79, 2924–2932. <https://pubs.acs.org/doi/10.1021/acs.jnatprod.6b00733>.
- Yang, Y., Xiang, K., Sun, D., Zheng, M., Song, Z., Li, M., Wang, X., Li, H., Chen, L., 2021. Withanolides from dietary tomatillo suppress HT1080 cancer cell growth by targeting mutant IDH1. *Bioorg. Med. Chem.* 36, 116095. <https://doi.org/10.1016/j.bmc.2021.116095>.
- Zhang, D.Y., Lou, H.Y., Chen, C., Liu, H.F., Zhang, N., Deng, C.Y., Li, J.Y., Pan, W.D., 2022. Cipacinerasins A–K, structurally diverse limonoids from *Cipadessa baccifera*. *Phytochemistry* 200, 113186. <https://doi.org/10.1016/j.phytochem.2022.113186>.
- Zhang, H.P., Wu, S.H., Shen, Y.M., Ma, Y.B., Wu, D.G., Qi, S.H., Luo, X.D., 2003. A pentanortriterpenoid with a novel carbon skeleton and a new pregnane from *Trichilia connaroides*. *Can. J. Chem.* 81, 253–257. <https://doi.org/10.1139/V03-025>.
- Zhou, Z.F., Kurtán, T., Mandi, A., Gu, Y.C., Yao, L.G., Xin, G.R., Li, X.W., Guo, Y.W., 2016. Novel and neuroprotective tetranortriterpenoids from Chinese mangrove *Xylocarpus granatum* Koenig. *Sci. Rep.* 6, 33908. <https://doi.org/10.1038/srep33908>.
- Zhu, G.L., Wan, L.S., Peng, X.R., Shi, Q.Q., Li, X.N., Chen, J.C., Zhou, L., Qiu, M.H., 2019. Cytotoxic limonoids from the twigs and leaves of *Toona ciliata*. *J. Nat. Prod.* 82, 2419–2429. <https://doi.org/10.1021/acs.jnatprod.8b00954>.